CHAPTER 5

ANALYSIS OF SIZE EFFECTS ON THERMOELASTIC DAMPING IN THE KIRCHHOFF'S PLATE RESONATOR UNDER MOORE-GIBSON-THOMPSON THERMOELASTICITY

5.1 Introduction[1]

Extensive research work carried out during last several decades has indicated that Kirchhoff plate resonator is widely applicable to have ultra-high resonant frequency. Due to their excellent characteristics, Kirchhoff's plate resonators have a wide range of possible applications in the rapidly expanding nanotechnology sector. The rectangular plate is one of the most important structures for sensors and resonators in the precise estimation of thermoelastic damping (TED) response. Therefore, the study of such structures has drawn significant attention of researchers as it is critical to understand the behavior of these micro/nanostructures with reasonable accuracy.

There have been some investigations of TED addressing microplate resonators in the recent past. Guo et al. (2012) used the non-classical heat conduction model of the dual-phase-lag (DPL) to derive an explicit formula for TED in micro plate. Zhong et al. (2014) proposed the TED formulation for an entirely simply supported micro

[1]The content of this chapter is published in **Thin-Walled Structures**, 180, 2022.

plate resonator to get the closed-form solution of equation for TED. Based on the MCST, Razavilar et al. (2016) investigated the effect of the length scale parameter on the TED in a rectangular micro plate. Kumar et al. (2017) examined the vibrations analysis in circular plate resonators for thermoelastic medium under LS thermoelasticity theory. Borjalilou et al. (2018) developed a closed-form relation for analyzing TED in Kirchhoff plates using the MCST and DPL heat conduction model. Devi and Kumar (2018) investigated the thermoelastic damping and frequency shift in Kirchhoff micro plate resonators using the DPL heat conduction model. Borjalilou and Asghari (2019) also performed an investigation using the DPL model to evaluate the size effect on TED in Kirchhoff rectangular micro plates. Kumar and Mukhopadhyay (2020) utilized MCST and the three-phase-lag (TPL) (2007) heat conduction model to find a closed-form expression for TED in thin rectangular micro plates. Wang et al. (2022) derived the analytical solution of viscoelastic nanoplate to capture bending analysis based on MCST.

From the literature review and the author's knowledge, TED analysis of Kirchhoff micro plate resonators based on MCST under new heat conduction model (MGT model) has not been reported previously. This topic is therefore covered extensively in the current chapter of the thesis. The main contribution of this chapter is therefore to examine the damping behavior of a Kirchhoff's micro plate resonator by taking into consideration the MCST as non-classical continuum theory for the study of size effects. Hamilton's principle is used in conjunction with the modified couple stress and Kirchhoff plate theories to derive governing equations of motion based on the MGT thermoelasticity theory. An explicit expression for determining TED in a microplate resonator is established by solving these coupled equations, including small-scale effects. The thermoelastic damping and frequency shift diagrams for various parameters are also depicted to assess the behavior of the microplate resonator in the present context.

5.2 Dynamic Model of Rectangular Micro-plate

The geometric aspect and coordinate representation ($0 \leqslant x \leqslant a,\ 0 \leqslant y \leqslant b,\ -h/2 \leqslant z \leqslant h/2$) of a rectangular micro-plate resonator with length a, width b and uniform micro plate thickness h based on plane stress condition is considered as delineated in Fig. 5.2.1. To examine TED in Kirchhoff plate model (Reddy (1999)), the displacement components are expressed as

$$u_x = -z\frac{\partial w\left(x,y,t\right)}{\partial x},\ u_y = -z\frac{\partial w\left(x,y,t\right)}{\partial y},\ u_z = w\left(x,y,t\right), \tag{5.2.1}$$

where $w\left(x,y,t\right)$ indicates the transverse deflection of the micro-plate at time t.

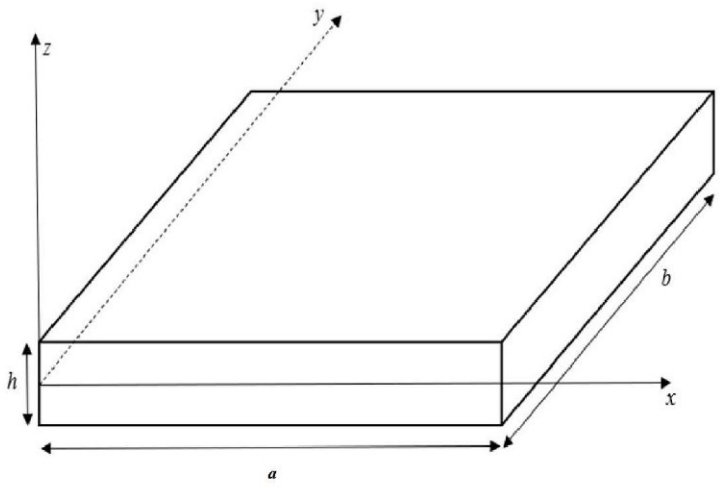

Figure 5.2.1: The geometric view and coordinate representation of a rectangular micro-plate resonator.

5.2.1 The Moore-Gibson-Thomson (MGT) thermoelasticity theory

In view of the MGT thermoelasticity theory, the heat conduction equation for isotropic material is expressed as

$$K\nabla^2\frac{\partial\theta}{\partial t}+K^*\nabla^2\theta=\left(1+\tau_q\frac{\partial}{\partial t}\right)\left(\rho c_E\frac{\partial^2\theta}{\partial t^2}+T_0\beta\,\frac{\partial^2 e_{kk}}{\partial t^2}\right), \tag{5.2.2}$$

where $\beta=\frac{E\alpha_t}{(1-2\vartheta)}$ is the thermoelastic coupling parameter under the present theory. Above equation under MGT thermoelasticity theory can extract the corresponding equations of the LS and GN-III thermoelasticity theories as follows:

- **LS thermoelasticity theory:** when $K^*=0$, $\tau_q\neq 0$.
- **GN-III thermoelasticity theory:** when $K^*\neq 0$,$\tau_q=0$.

5.3 Governing Equations of Rectangular Micro-plate Resonator

The equation of motion in terms of deflection function, the variation in the strain energy U_s for the Kirchhoff's plate theory in the present context take the following form:

$$U_s=\int_0^a\int_0^b\left[(\sigma_{xx}e_{xx}+\sigma_{yy}e_{yy}+2\sigma_{xy}e_{xy})+(\Upsilon_{xx}\chi_{xx}+\Upsilon_{yy}\delta\chi_{yy}+\Upsilon_{xy}\chi_{xy})\right]dxdy, \tag{5.3.1}$$

where the nonzero strain and symmetric part of the rotation gradient tensors can be defined as follows:

$$e_{xx}=-z\frac{\partial^2 w}{\partial x^2},\quad e_{yy}=-z\frac{\partial^2 w}{\partial y^2},\quad e_{xy}=-z\frac{\partial^2 w}{\partial x\partial y}, \tag{5.3.2}$$

$$\chi_{xx}=\frac{\partial^2 w}{\partial x\partial y},\quad \chi_{yy}=-\frac{\partial^2 w}{\partial x\partial y},\quad \chi_{xy}=\frac{1}{2}\left[\frac{\partial^2 w}{\partial y^2}-\frac{\partial^2 w}{\partial x^2}\right]. \tag{5.3.3}$$

By putting the Eqs. (5.3.2) and (5.3.3) into Eq. (5.3.1), the variation of strain energy function can be written as

$$U_s = \int_0^a \int_0^b \left\{ -N_{xx}\left(\frac{\partial^2 w}{\partial x^2}\right) - N_{yy}\left(\frac{\partial^2 w}{\partial y^2}\right) - 2N_{xy}\left(\frac{\partial^2 w}{\partial x \partial y}\right) \right\} + \left\{ P_{xx}\left(\frac{\partial^2 w}{\partial x \partial y}\right) - P_{yy}\left(\frac{\partial^2 w}{\partial x \partial y}\right) + P_{xy}\left(\frac{\partial^2 w}{\partial y^2}\right) - P_{xy}\left(\frac{\partial^2 w}{\partial x^2}\right) \right\} dxdy, \tag{5.3.4}$$

where

$$N_{xx} = \int_{-h/2}^{h/2} \sigma_{xx} z dz, \quad N_{yy} = \int_{-h/2}^{h/2} \sigma_{yy} z dz, \quad N_{xy} = \int_{-h/2}^{h/2} \sigma_{xy} z dz, \tag{5.3.5}$$

$$P_{xx} = \int_{-h/2}^{h/2} \Upsilon_{xx} dz, \quad P_{yy} = \int_{-h/2}^{h/2} \Upsilon_{yy} dz, \quad P_{\mathrm{xy}} = \int_{-h/2}^{h/2} \Upsilon_{xy} dz. \tag{5.3.6}$$

In Eqs. (5.3.5) and (5.3.6), the components N_{xx}, N_{yy} and N_{xy} are stress resultants. In addition, the components P_{xx}, P_{yy} and P_{xy} denote couple stress resultants.
The variation of kinetic energy $\left(\hat{\Upsilon}_{K.E}\right)$ of the plate without taking into account rotating inertia is decribed as (see Guo et al. (2012))

$$\delta\left(\hat{\Upsilon}_{K.E}\right) = \rho h \int_0^a \int_0^b \frac{\partial w}{\partial t} \delta\left(\frac{\partial w}{\partial t}\right) dxdy. \tag{5.3.7}$$

Now, in order to obtain the governing equation of the motion and the related boundary conditions of the plate, the application of the generalized Hamilton's principle (Dym (1973)) is defined on the time interval $[t_1, t_2]$ as follows:

$$\delta \int_{t_1}^{t_2} \left(U_s - \hat{\Upsilon}_{K.E}\right) dt = 0. \tag{5.3.8}$$

Introducing Eqs. (5.3.4) and (5.3.7) into Hamilton's principle, the following governing equation of the motion is obtained:

$$\frac{\partial^2 N_{xx}}{\partial x^2} + 2\frac{\partial^2 N_{xy}}{\partial x \partial y} + \frac{\partial^2 N_{yy}}{\partial y^2} - \frac{\partial^2 P_{xx}}{\partial x \partial y} + \frac{\partial^2 P_{xy}}{\partial x^2} - \frac{\partial^2 P_{xy}}{\partial y^2} + \frac{\partial^2 P_{yy}}{\partial x \partial y} = \rho h \frac{\partial^2 w}{\partial t^2} \tag{5.3.9}$$

with the pertinent boundary conditions as

$$\delta w = 0 \quad \text{or} \quad \left(\frac{\partial N_{xx}}{\partial x} + \frac{\partial N_{xy}}{\partial y} - \frac{1}{2}\frac{\partial P_{xx}}{\partial y} + \frac{\partial P_{xy}}{\partial x} + \frac{1}{2}\frac{\partial P_{yy}}{\partial y}\right) n_x + \left(\frac{\partial N_{xy}}{\partial x} + \frac{\partial N_{yy}}{\partial y} - \frac{1}{2}\frac{\partial P_{xx}}{\partial x} - \frac{\partial P_{xy}}{\partial y} + \frac{1}{2}\frac{\partial P_{yy}}{\partial x}\right) n_y = 0, \quad (5.3.10)$$

$$\delta\left(\frac{\partial w}{\partial x}\right) = 0 \quad \text{or} \quad N_{xx} + P_{xy} = 0 \quad \text{at } x = 0, \text{a}, \quad (5.3.11)$$

and

$$\delta\left(\frac{\partial w}{\partial y}\right) = 0 \quad \text{or} \quad N_{yy} - P_{xy} = 0 \quad \text{at y=0, b}, \quad (5.3.12)$$

where n_x and n_y are the components of unit normal vector to the boundary of rectangular plate.

The material is taken to be under plane stress condition assuming $\sigma_{zz} = 0$. The relation between the non-zero components of the Cauchy stress tensor and axial strain are obtained as

$$\sigma_{xx} = \frac{E}{(1-\vartheta^2)}\left(e_{xx} + \vartheta e_{yy}\right) - \frac{1}{1-\vartheta} E\alpha_t\theta, \quad (5.3.13)$$

$$\sigma_{yy} = \frac{E}{(1-\vartheta^2)}\left(e_{yy} + \vartheta e_{xx}\right) - \frac{1}{1-\vartheta} E\alpha_t\theta, \quad (5.3.14)$$

$$e_{zz} = -\frac{\vartheta}{(1-\vartheta)}\left(e_{xx} + e_{yy}\right) + \frac{1+\vartheta}{1-\vartheta}\alpha_t\theta. \quad (5.3.15)$$

By introducing Eq. (5.3.2) into Eqs. (5.3.13) – (5.3.15), it is found that

$$\sigma_{xx} = -\frac{Ez}{(1-\vartheta^2)}\left(\frac{\partial^2 w}{\partial x^2} + \vartheta\frac{\partial^2 w}{\partial y^2}\right) - \frac{1}{1-\vartheta} E\alpha_t\theta, \quad (5.3.16)$$

$$\sigma_{yy} = -\frac{Ez}{(1-\vartheta^2)}\left(\frac{\partial^2 w}{\partial y^2} + \vartheta\frac{\partial^2 w}{\partial x^2}\right) - \frac{1}{1-\vartheta} E\alpha_t\theta, \quad (5.3.17)$$

$$e_{zz} = \frac{\vartheta z}{(1-\vartheta)}\left(\frac{\partial^2 w}{\partial x^2} + \frac{\partial^2 w}{\partial y^2}\right) + \frac{1+\vartheta}{1-\vartheta}\alpha_t\theta. \quad (5.3.18)$$

When Eqs. (5.3.3), (5.3.5), (5.3.6), (5.3.16) and (5.3.17) are combined, the stress resultants in terms of plate deflection in the thermoelastic condition are given as follows:

$$\begin{bmatrix} N_{xx} \\ N_{yy} \\ N_{xy} \end{bmatrix} = -\Lambda \begin{bmatrix} 1 & \vartheta & 0 \\ \vartheta & 1 & 0 \\ 0 & 0 & 1-\vartheta \end{bmatrix} \begin{bmatrix} w_{xx} \\ w_{yy} \\ w_{xy} \end{bmatrix} - \frac{1}{1-\vartheta} \begin{bmatrix} N_T \\ N_T \\ 0 \end{bmatrix}, \tag{5.3.19}$$

$$\begin{bmatrix} P_{xx} \\ P_{yy} \\ P_{xy} \end{bmatrix} = \mu l^2 h \begin{bmatrix} 0 & 0 & 2 \\ 0 & 0 & -2 \\ -1 & 1 & 0 \end{bmatrix} \begin{bmatrix} w_{xx} \\ w_{yy} \\ w_{xy} \end{bmatrix}, \tag{5.3.20}$$

where $\Lambda = \frac{1}{12} E h^3 \frac{1}{(1-\vartheta^2)}$ and $N_T = E\alpha_t \int_{-h/2}^{h/2} \theta z dz$ denote the bending rigidity and thermal moments, respectively.

Therefore, the equation of motion is expressed in terms of the deflection function w by substituting Eqs. (5.3.19) and (5.3.20) into Eq. (5.3.9) as

$$(\Lambda + \mu l^2 h)\left(\frac{\partial^4 w}{\partial x^4} + 2\frac{\partial^4 w}{\partial x^2 \partial y^2} + \frac{\partial^4 w}{\partial y^4}\right) + \frac{1}{1-\vartheta}\left(\frac{\partial^2 N_T}{\partial x^2} + \frac{\partial^2 N_T}{\partial y^2}\right) + \rho h \frac{\partial^2 w}{\partial t^2} = 0. \tag{5.3.21}$$

The above equation can be mainly characterized by three parts: the first part with Λ and ρh reflects the conventional plate model; the second part with $\mu l^2 h$ exhibits the size-effect and the third part with N_T represents the thermoelastic coupling effect. Furthermore, by setting $l = 0$, this new model reduces to the conventional thermoelastic plate model, which ignores the size impact. Some researchers have previously shown that temperature gradients in thin plates along the z-direction are substantially more considerable than gradients in the x and y directions (Lifshitz and Roukes (2000)). Therefore, it is permissible to examine one-dimensional heat conduction. The term of $\nabla^2\theta$ in the Eq. (5.2.2) can therefore be replaced by $\frac{\partial^2\theta}{\partial z^2}$. Thus, the Eq. (5.2.2) yields

$$\left(K\frac{\partial}{\partial t}+K^{*}\right)\frac{\partial^{2}\theta}{\partial z^{2}}=\left(1+\tau_{q}\frac{\partial}{\partial t}\right)\left(\rho c_{E}\frac{\partial^{2}\theta}{\partial t^{2}}+T_{0}\beta\,\frac{\partial^{2}e_{kk}}{\partial t^{2}}\right). \tag{5.3.22}$$

By substituting the components of volumetric strain, i.e. (e_{xx}, e_{yy} and e_{zz}) into the Eq. (5.3.22), one can obtain

$$\Omega\left(\frac{\partial}{\partial t}+\frac{K^{*}}{K}\right)\frac{\partial^{2}\theta}{\partial z^{2}}=\left(1+\tau_{q}\frac{\partial}{\partial t}\right)\left(1+\frac{2\triangle_{E}\left(1+\vartheta\right)}{\left(1-\vartheta\right)\left(1-2\vartheta\right)}\right)\left[\frac{\partial^{2}\theta}{\partial t^{2}}-\frac{\triangle_{E}z}{\alpha_{t}}\left(\frac{\partial^{4}w}{\partial x^{2}\partial t^{2}}+\frac{\partial^{4}w}{\partial y^{2}\partial t^{2}}\right)\right], \tag{5.3.23}$$

where $\Omega=\frac{K}{\rho c_{E}}$ and $\triangle_{E}=\frac{E\alpha_{t}^{2}T_{0}}{\rho c_{E}}$ denote the thermal diffusivity and relaxation strength of the material, respectively. The relation can be simplified due to the low amount of relaxation strength (*i.e.*, $\triangle_{E}\ll 1$). Hence, the following is the final version of the energy equation:

$$\Omega\left(\frac{\partial}{\partial t}+\frac{K^{*}}{K}\right)\frac{\partial^{2}\theta}{\partial z^{2}}+\left(1+\tau_{q}\frac{\partial}{\partial t}\right)\frac{\triangle_{E}z}{\alpha_{t}}\left(\frac{\partial^{4}w}{\partial x^{2}\partial t^{2}}+\frac{\partial^{4}w}{\partial y^{2}\partial t^{2}}\right)=\left(1+\tau_{q}\frac{\partial}{\partial t}\right)\frac{\partial^{2}\theta}{\partial t^{2}}. \tag{5.3.24}$$

5.4 Quality Factor (QF) of TED

In a micro resonator, less energy dissipation, enhanced stability, and increased sensitivity are all benefits of a high QF. In order to obtain the expression of QF in the present context, the coupled thermoelastic equations are considered to have simple-harmonic vibrations to identify the effect of thermoelastic coupling as follows:

$$w\left(x,y,t\right)=W_{0}\left(x,y\right)\ \exp\ \left(i\omega t\right),\quad \theta\left(x,y,z,t\right)=\Theta_{0}\left(x,y,z\right)\ \exp\ \left(i\omega t\right), \tag{5.4.1}$$

where W_0 indicates the mechanical amplitude, Θ_0 is the temperature distribution in the micro plate. ω is an angular frequency per cycle of vibration.

In view of the Eqs. (5.3.24) and (5.4.1), the following form is obtained:

$$\frac{\partial^2\Theta_0}{\partial z^2}+g^2\Theta_0=g^2\frac{\triangle_E}{\alpha_t\left(1-\vartheta\right)}z\left(\frac{\partial^2 W_0}{\partial x^2}+\frac{\partial^2 W_0}{\partial y^2}\right), \tag{5.4.2}$$

in which

$$g^2=\frac{\omega}{\Omega}\frac{\left(\omega+i\omega^2\right)}{\left(\frac{K^*}{K}+i\omega\right)}.$$

The complex parameter g can be expressed as follows:

$$g=\sqrt{\frac{\omega}{\Omega}}\sqrt{\beta_1-i\beta_2}=\frac{\xi}{h}\left(\xi_1-i\frac{\beta_2}{\xi_1}\right), \tag{5.4.3}$$

where

$$\begin{aligned}&\xi=h\sqrt{\frac{\omega}{2\Omega}},\quad \xi_1=\sqrt{\sqrt{\beta_1^2+\beta_2^2}+\beta_1},\\ &\beta_1=\omega\frac{\left(\frac{K^*}{K}+\tau_q\omega^2\right)}{\left\{\left(\frac{K^*}{K}\right)^2+\omega^2\right\}},\quad \beta_2=\omega\frac{\left(1-\tau_q\frac{K^*}{K}\right)\omega}{\left\{\left(\frac{K^*}{K}\right)^2+\omega^2\right\}}.\end{aligned} \tag{5.4.4}$$

The general solution of Eq. (5.4.2) for the unknown function Θ_0 is derived as

$$\Theta_0\left(x,y,z\right)=A_1\sin\left(gz\right)+A_2\cos\left(gz\right)+\frac{\triangle_E}{\alpha_t\left(1-\vartheta\right)}z\left(\frac{\partial^2 W_0}{\partial x^2}+\frac{\partial^2 W_0}{\partial y^2}\right), \tag{5.4.5}$$

where $A_i\,(i=1,2)$ are arbitrary coefficients. These unknown coefficients A_1 and A_2 can be found out by applying thermal boundary conditions at the top and the adiabatic base surfaces of the micro plate. Many elements, including environmental temperature, structural size, material properties, boundary conditions, resonance frequencies, and so on, affect the practical micro/nano scale thermoelastic problems, making them exceed-

ingly complex. The heat flux between the surfaces and surroundings of the micro/nano structures is adequately small. Therefore, the adiabatic boundary conditions on both surfaces are taken as follows

$$\frac{\partial \Theta_0}{\partial z} = 0 \text{ at } \begin{cases} z = h/2 \\ \\ z = -h/2 \end{cases} . \tag{5.4.6}$$

In view of the Eq. (5.4.6), the temperature distribution in the micro-plate is obtained as

$$\Theta_0 (x, y, z) = \frac{\triangle_E}{\alpha_t \, (1 - \vartheta)} z \left(\frac{\partial^2 W_0}{\partial x^2} + \frac{\partial^2 W_0}{\partial y^2} \right) \left[z - \frac{\sin (gz)}{z \cos \left(\frac{gh}{2} \right)} \right] . \tag{5.4.7}$$

Using Eqs. (5.3.21), (5.4.1) and (5.4.7), the equation of motion takes form as

$$\rho h \omega^2 W_0 = \left\{ \Lambda + \mu l^2 h + \frac{E h^3}{12 \left(1 - \vartheta\right)^2} \triangle_E \left(1 + f(\omega)\right) \right\} \left(\frac{\partial^4 W_0}{\partial x^4} + 2 \frac{\partial^4 W_0}{\partial x^2 \partial y^2} + \frac{\partial^4 W_0}{\partial y^4} \right) . \tag{5.4.8}$$

Here $f(\omega)$ is a complex valued function, which is derived as

$$f \left(\omega\right) = \frac{24}{h^3 g^3} \left\{ \frac{hg}{2} - \tan \left(\frac{hg}{2} \right) \right\} . \tag{5.4.9}$$

When the thermoelastic coupling is ignored, i.e., $(\triangle_E = 0)$, then the Eq. (5.4.8) reduces to the form in the isothermal case as

$$\rho h \omega_0^2 W_0 = \left(\Lambda + \mu l^2 h \right) \left(\frac{\partial^4 W_0}{\partial x^4} + 2 \frac{\partial^4 W_0}{\partial \mathrm{x}^2 \partial y^2} + \frac{\partial^4 W_0}{\partial y^4} \right) , \tag{5.4.10}$$

where ω_0 indicates the isothermal frequency. In the case of isothermal conditions, it is sufficient to set the thermal expansion coefficient α_t equal to zero.

By using the Eqs. (5.4.8) and (5.4.10), the coupling between ω and ω_0 is acquired as follows:

$$\omega = \omega_0 \sqrt{1 + \frac{\left(\frac{1+\vartheta}{1-\vartheta}\right) \triangle_E \left(1 + f(\omega)\right)}{P}}, \tag{5.4.11}$$

where P represents the ratio of bending rigidity which is defined as

$$P = 1 + 6\left(1 - \vartheta\right)\left(\frac{l}{h}\right)^2.$$

It is well known that ω_0 depends at supporting boundary conditions of plate. Thereafter, the simply supported (SS) boundary condition can be implemented at all four edges of micro plate. Moreover, the admissible deflection function can be taken as:

$$W_0\left(x, y\right) = \sum_{m=1}^{\infty}\sum_{n=1}^{\infty} \Psi_{mn} \sin\left(\frac{m\pi}{a}\mathrm{x}\right) \sin\left(\frac{n\pi}{b}y\right), \tag{5.4.12}$$

where Ψ_{mn}, $(m, n = 1, 2, ..)$ is constant. Here, m and n represent the modes of vibration. Substituting Eqs. (5.4.12) into (5.4.10), the following expression is found for ω_0:

$$\omega_0 = \pi^2 \sqrt{\frac{\Lambda + \mu l^2 h}{\rho h}} \left(\left(\frac{m}{a}\right)^2 + \left(\frac{n}{b}\right)^2\right). \tag{5.4.13}$$

As it is well known that the amount of relaxation strength $\triangle_E$ is very less i.e., $(\triangle_E \ll 1)$, hence, expanding Eq. (5.4.11) using Taylor's series and neglecting the higher order terms of $\triangle_E$, it is obtained that

$$\omega = \omega_0 \left\{1 + \frac{\left(\frac{1+\vartheta}{1-\vartheta}\right) \triangle_E \left(1 + f(\omega)\right)}{2P}\right\}. \tag{5.4.14}$$

In view of the insignificant discrepancy between the magnitude of real and imaginary parts of $f(\omega)$ and $f(\omega_0)$, we can rewrite $f(\omega)$ by $f(\omega_0)$ as follows:

$$\omega = \omega_0 \left\{1 + \frac{\left(\frac{1+\vartheta}{1-\vartheta}\right) \triangle_E \left(1 + f(\omega_0)\right)}{2P}\right\}. \tag{5.4.15}$$

In the end, the real and imaginary parts of the angular frequency ω can be determined

as follows:

$$Re(\omega) = \omega_0 \left[1 + \frac{1+\vartheta}{2(1-\vartheta)} \frac{\triangle_E}{P} \left\{ 1 + 12 \frac{\left(\xi_1^2 - \frac{\beta_2^2}{\zeta^2}\right)}{\xi^2 \left(\xi_1^2 + \frac{\beta_2^2}{\xi_1^2}\right)^2} , \right. \right.$$
$$\left. \left. -24 \frac{\left(\xi_1^3 - 3\frac{\beta_2^2}{\xi_1}\right) \sin(\xi\xi_1) + \left(3\xi_1\beta_2 - \frac{\beta_2^3}{\xi_1^3}\right) \sinh\left(\frac{\xi\beta_2}{\xi_1}\right)}{\xi^3 \left(\xi_1^2 + \frac{\beta_2^2}{\xi_1^2}\right)^3 \left(\cos(\xi\xi_1) + \cosh\left(\frac{\xi\beta_2}{\xi_1}\right)\right)} \right\} \right], \tag{5.4.16}$$

$$Im(\omega) = \omega_0 \frac{12(1+\vartheta)}{(1-\vartheta)} \frac{\triangle_E}{P} \left[\frac{\beta_2}{\xi^2 \left(\xi_1^2 + \frac{\beta_2^2}{\xi_1^2}\right)^2} \right.$$
$$\left. - \frac{\left(3\xi_1\beta_2 - \frac{\beta_2^3}{\xi_1^3}\right) \sin(\xi\xi_1) - \left(\xi_1^3 - 3\frac{\beta_2^2}{\xi_1}\right) \sinh\left(\frac{\xi\beta_2}{\xi_1}\right)}{\xi^3 \left(\xi_1^2 + \frac{\beta_2^2}{\xi_1^2}\right)^3 \left(\cos(\xi\xi_1) + \cosh\left(\frac{\xi\beta_2}{\xi_1}\right)\right)} \right]. \tag{5.4.17}$$

Furthermore, the normalized frequency shift and normalized attenuation can be expressed in terms of the real and imaginary parts of ω as

$$\text{Normalized frequency shift} = \frac{[Re(\omega) - \omega_0]}{\omega_0 \triangle_E}, \tag{5.4.18}$$

$$\text{Normalized attenuation} = \frac{Im(\omega)}{\omega_0 \triangle_E}. \tag{5.4.19}$$

In term of the inverse QF, the quantity of TED is given by

$$Q^{-1} = 2 \left| \frac{Im(\omega)}{Re(\omega)} \right|. \tag{5.4.20}$$

In view of the Eqs. (5.4.16) and (5.4.17), the analytical expression of inverse quality factor utilizing MCST and MGT thermoelasticity theory for Kirchhoff's micro plate resonator is finally obtained as follows:

$$Q^{-1} = \frac{24(1+\vartheta)}{(1-\vartheta)} \frac{\triangle_E}{P} \left[\frac{\beta_2}{\xi^2 \left(\xi_1^2 + \frac{\beta_2^2}{\xi_1^2}\right)^2} - \frac{\left(3\xi_1\beta_2 - \frac{\beta_2^3}{\xi_1^3}\right) \sin(\xi\xi_1) - \left(\xi_1^3 - 3\frac{\beta_2^2}{\xi_1}\right) \sinh\left(\frac{\xi\beta_2}{\xi_1}\right)}{\xi^3 \left(\xi_1^2 + \frac{\beta_2^2}{\xi_1^2}\right)^3 \left(\cos(\xi\xi_1) + \cosh\left(\frac{\xi\beta_2}{\xi_1}\right)\right)} \right]. \tag{5.4.21}$$

5.5 Results and Discussion

This section illustrates the analytical results of the present problem with suitable example and investigates the thermoelastic damping (TED) behavior in Kirchhoff's plate resonator. It attempts to evaluate the size dependency effects in the present context in details. Furthermore, detailed numerical observations are given for frequency shift analysis and the normalized attenuation based on four different materials (copper, gold, silicon, and lead). Table 5.1 shows the mechanical and thermal properties of four different types of materials (Devi and Kumar (2018), Tzou (2014)). The study of some parameters, such as microplate thickness, mode of vibration, aspect ratio, relaxation time parameter, and material type, are explored to understand their effects on the quality factor/TED in the present context.

Material and thermal properties	**Gold** (Au)	**Silicon** (**Si**)	**Copper** (Cu)	**Lead** (Pb)
Young's modulus E (GPa)	79	169	110	16
Poission's ratio ϑ	0.40	0.22	0.35	0.44
density $\rho\,(\mathrm{kgm}^{-3})$	19,300	2330	8940	11,340
Thermal conductivity $K\,(\mathrm{Wm}^{-1}\mathrm{K}^{-1})$	315	70	386	35.3
Thermal conductivity rate $K^*\,(\mathrm{Wm}^{-1}\mathrm{K}^{-1}\mathrm{s}^{-1})$	150	157	70	150
Specific heat $c_E\,(\mathrm{Jkg}^{-1}\mathrm{K}^{-1})$	129.1	713	385.9	128
Thermal expension coefficient $\alpha_t\ (10^{-6}\mathrm{K}^{-1})$	14.2	2.6	16.5	28.9

Table 5.1: The material and thermal properties at 300 K.

5.5.1 Analysis of thermoelastic attenuation and frequency shift

Figs. 5.5.1(a,b,c,d) show the graphical depiction of the normalized frequency shift and normalized attenuation in rectangular microplate resonators along with the dimensionless variable ξ for four different materials as mentioned above. Here, the dimensions of the microplate resonator are fixed by setting length $a = 50\,\mu m$ and width $b = 30\,\mu m$. Figs. 5.5.1(a,b,c,d) are plotted for the constant microplate thickness $h = 6\,\mu m$, where

the value of phase-lag parameter is taken as $\tau_q = 0.388 \times 10^{-10}$s. By observing the Figs. 5.5.1(a,b,c,d), the three main points can be summarized. Firstly, the behavior of normalized attenuation, which is the amount of dissipation of thermoelastic energy from the micro-plate resonator, first rises to a maximum at $\xi = 2.25$ and then declines concerning dimensionless variable ξ. Secondly, the intersecting point between the normalized frequency shift and normalized attenuation can be seen at the same point near $\xi = 2.25$ in cases of all four structural materials universally. The same observation has been found in the literature (Borjalilou and Asghari (2019), Resmi et al. (2021)) for other thermoelastic models. Lastly, it has been founded that as the frequency shift diminishes, attenuation reduces as well, causing an increase in the quality factor. In the current work, the order of Lead (Pb) > Gold (Au) > Copper (Cu) > Silicon (Si) is determined as the material order in which attenuation and frequency shift decrease with the function of ξ.

By neglecting the size effect ($l = 0$), the Fig. 5.5.2 shows the discrepancy in normalized attenuation for four different materials. In this numerical manipulation, the plate thickness $h = 5\mu m$ and relaxation parameter $\tau_q = 0.388 \times 10^{-10}$s are adopted. It is noticeable that the normalized attenuation of the microplate resonator increases first before reaching a maximum value of TED, then decreases with increasing ξ after its peak. As it is clear that the maximum rate of thermoelastic energy dissipation is found for lead material and silicon-based material resonators exhibit the slowest rate of thermoelastic energy dissipation. The statistics depict that the variety of materials significantly affects the vibrational response of microplate resonators when ξ increases. Furthermore, it has been discovered that a resonator composed of silicon will have a longer time of vibration response.

Fig. 5.5.3 shows a frequency shift analysis as a function of normalized frequency ξ for different materials with a fixed length scale parameter $l = 1\mu m$. The obtained results in Fig. 5.5.3 show that as the frequency shift diminishes, it causes an increase in the quality

factor in different materials in the order of Lead (Pb) > Gold (Au) > Copper (Cu) > Silicon (Si). Thus, the rate of energy dissipation (thermoelastic damping) will be higher for the resonator, which is composed of Lead (Pb).

Fig. 5.5.4 displays the influence of the internal material length scale parameter on frequency shift. Here, we plotted the nature of frequency shift for four different aspect ratios with l, by fixing $l/h = 0, 0.1, 0.2, 0.3$. By setting the values of l, we found the variation of frequency shift for both theories (CCT and MCST) separately. It can be clearly seen that the impact of internal material length parameter l is prominent in the study of frequency shift. Furthermore, this is discovered that as the material length-scale parameter's ratio l/h is increased, the normalized frequency shift reduces dramatically. This discovered truth will be the primary reason for the high-quality factor and low energy dissipation during vibration. Moreover, it is found that the predicted size-dependent normalized frequency shifts are lower in MCST as compared to the CCT, which means that any alteration in material length scale parameter leads to lower values of frequency shift.

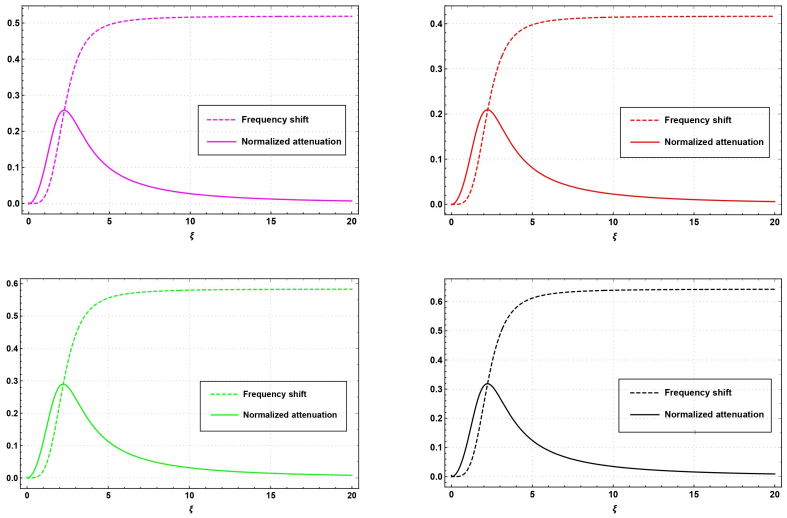

Figure 5.5.1: Comparison of normalized attenuation and frequency shift with respect to ξ at first mode $(1, 1)$ for four different materials (Cu,Si, Au and Pb).

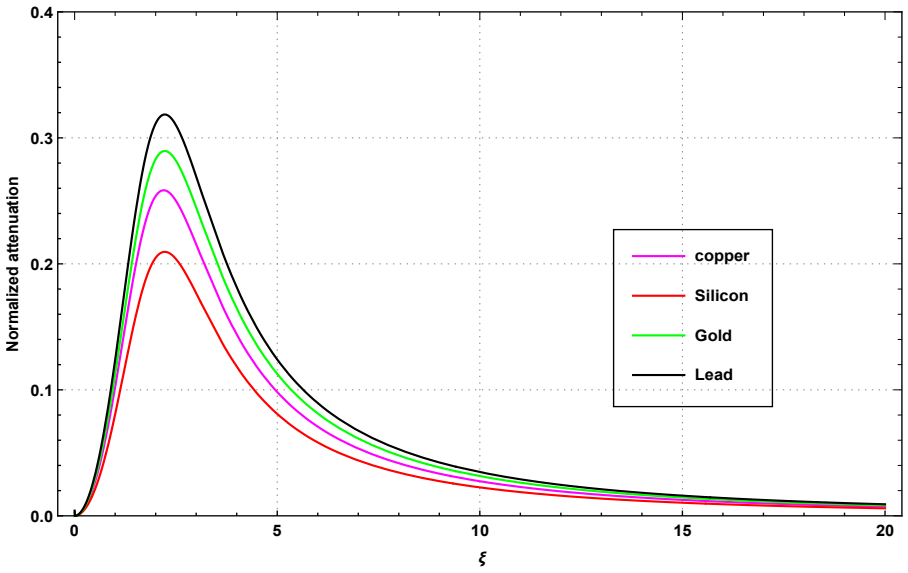

Figure 5.5.2: Comparison of normalized attenuation without considering small-scale effect ($l = 0$) for various materials.

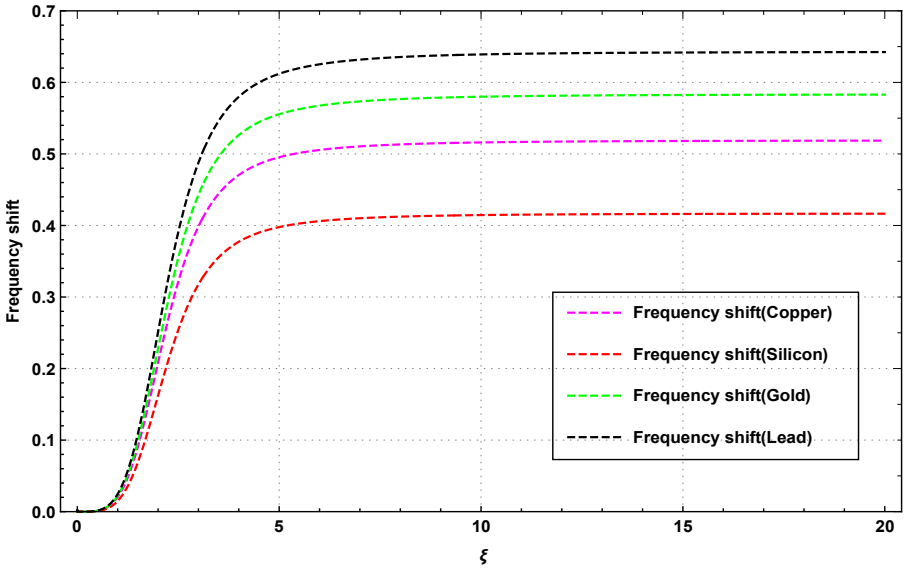

Figure 5.5.3: Comparison of frequency shift considering small-scale effect ($l = 1\mu m$) for various materials.

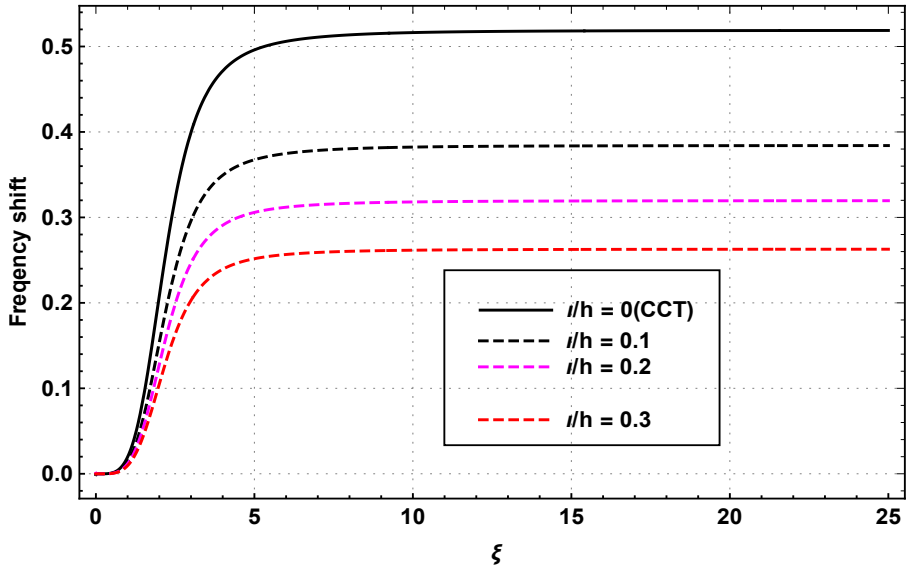

Figure 5.5.4: Comparison of frequency shift with respect to ξ at first mode $(1,1)$ for different aspect ratios of l/h.

5.5.2 Influence of material length-scale parameter on TED

To see the dominance of material length scale parameter on TED, Figs. 5.5.5(a,b) are plotted under the simply supported (SS) boundary conditions for the first mode $(1,1)$ and the second mode $(2,2)$ of vibration, respectively. Both figures illustrate the size-dependent TED with respect to a function of the normalized variable ξ for different aspect ratios ($l/h = 0, 0.1, 0.2,$ and 0.3). It has been revealed that MCST estimates lower damping values than the conventional continuum theory ($l = 0$). For both modes, it is witnessed that the TED increases initially and then converges to an equilibrium state after reaching its maximum peak value. It is also concluded that the resulting QF values predicted for the first mode are more significant than those obtained for the second mode. Hence, it can be worthy to say that rate of energy dissipation is much lesser at the first mode $(1,1)$.

By assuming the fixed values of normalized frequency $\xi = 2.25$ and dimensions of micro plate i.e., length $a = 50\,\mu m$ and width $b = 40\,\mu m$, the comparison of TED with the function of microplate thickness for first mode $(1,1)$ is illustrated in Fig. 5.5.6.

Fig. 5.5.6 demonstrates that the non-classical continuum theory (MCST) takes into consideration at lower TED values than the conventional continuum theory (CCT). It is shown that when MCST is used to determine the quality factor, the results are higher than when using the classical continuum theory. It is a significant finding of the current study and this emphasizes the importance of building an efficient plate resonator. Fig. 5.5.6 shows that the energy dissipation rate estimated under the current model is considerably higher when the material length scale parameter is small.

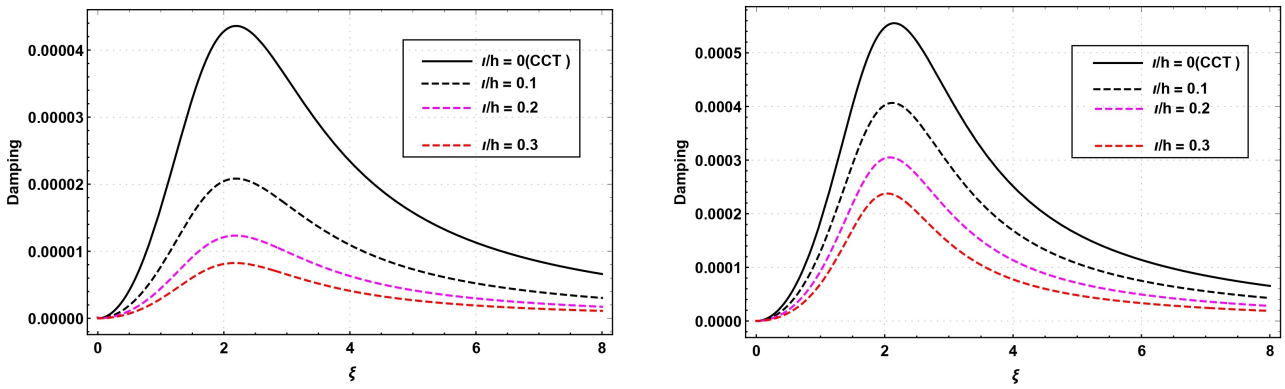

Figure 5.5.5: (a) Comparison of TED for first mode (1, 1). (b) Comparison of TED for ssecond mode $(2, 2)$.

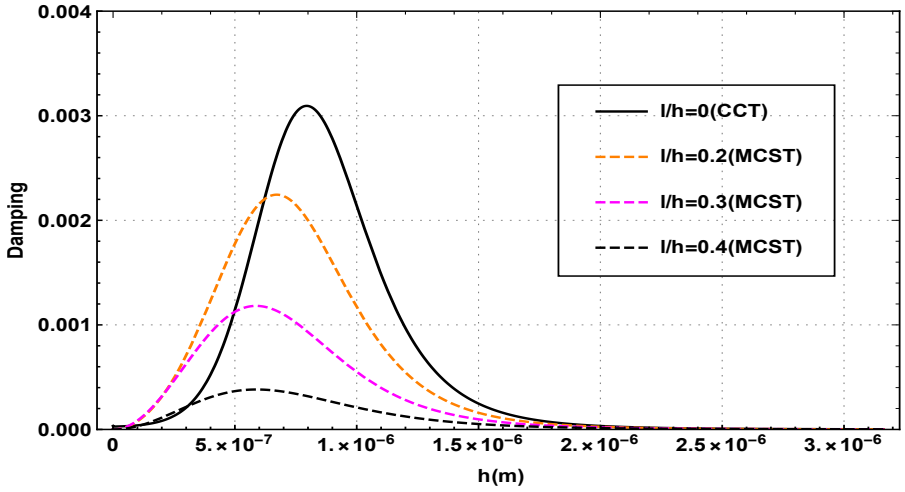

Figure 5.5.6: Comparison of TED values for CCT and MCST with different aspect ratios l/h along with first mode $(1, 1)$.

5.5.3 Effect of aspect ratios $(a/h,\ b/h)$ and dimensions of micro-plate on TED

Figs. 5.5.7(a,b) represent the influence of employing different aspect ratios on TED while keeping a constant micro plate width $b = 40\,\mu m$. The outcomes are based on fixed micro-plate thickness $h = 1\,\mu m$. The figures are plotted under the first and second modes, respectively. It's worth noting that when the aspect ratio a/h increases, the QF increases dramatically for both modes, but the peak value of TED declines. When comparing the first and second modes, it is noteworthy that the first mode indicates the most TED.

Fig. 5.5.8 depicts the discrepancy in TED as the function of plate thickness h for different values of length of microplate a ($a = 20\,\mu m$, $25\,\mu m$, $30\,\mu m$ and $35\,\mu m$). All curves are plotted under the fixed $b = 30\,\mu m$, and the material length parameter is assumed to be $l = 1\,\mu m$. It can be seen that as the length of micro plate is increased, the peak value of TED remains relatively consistent. Also, the peaks of TED are observed to be too sharp for higher values of the length of the plate resonator. It concludes that the resonator will have fewer vibration responses under a higher value of the microplate's length. So, this is a considerable reason for having a less quality factor at a higher value of the microplate's length.

Figs. 5.5.9(a,b) display the influence of employing distinct aspect ratios, ($b/h =$ 20,25,30 and and 35) on TED versus ξ while keeping a constant micro plate length $a = 50\,\mu m$. The effect of aspect ratios b/h is obtained in the context of first and second modes, separately. It is clear that when the microplate resonators are wider, the quality factor increases with both modes. When the aspect ratio b/h increases, the peak value of damping decreases significantly. Also, it has been observed that the energy dissipation rate is higher for the first mode as compared to the second mode.

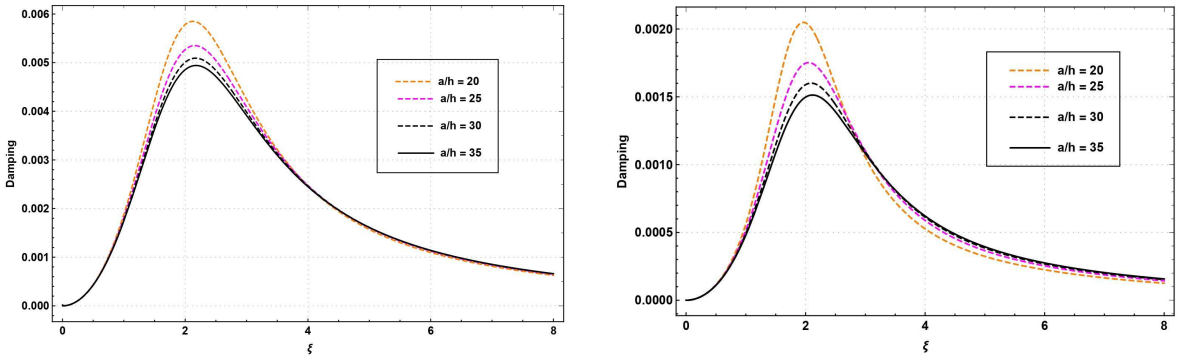

Figure 5.5.7: (a) Comparison of TED for different aspect ratios of $\frac{a}{h}$ corresponding to first mode. (b) Comparison of TED for different aspect ratios of $\frac{a}{h}$ corresponding to second mode.

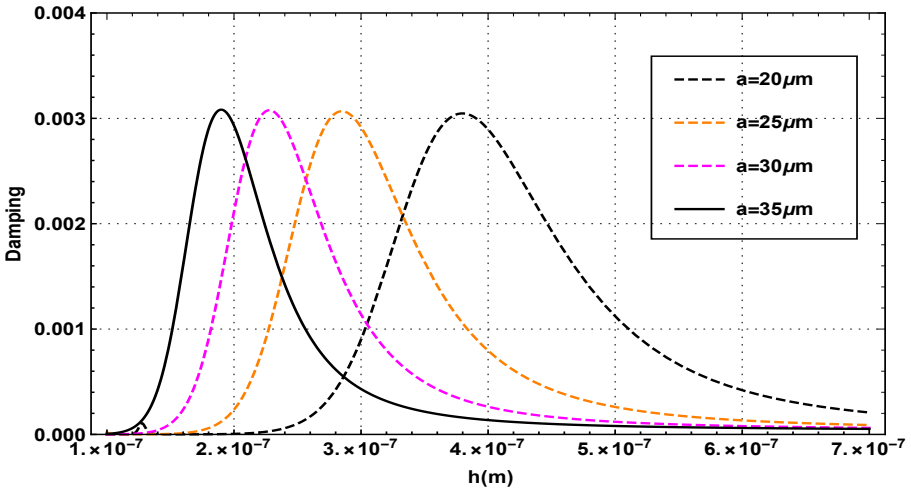

Figure 5.5.8: Comparison of TED along plate thickness for different values of length of plate a.

Fig. 5.5.10 depicts the variation of damping against a plate thickness h for distinct values of width of microplate b ($b = 20\,\mu m$, $25\,\mu m$, $30\,\mu m$ and $35\,\mu m$). By keeping a constant length scale parameter $l = 1\,\mu m$, the minimum and maximum of peak values are obtained under the fixed plate length $a = 50\,\mu m$. The peak value of TED grows significantly as the width of microplate b increases. Therefore, it implies that the rate of energy dissipation (TED) gets higher when the width of the microplate increases.

As a result, the quality factor prediction is lower for the larger width of microplate resonator. According to the finding mentioned earlier, better vibration responses can be achieved with a smaller width of a microplate.

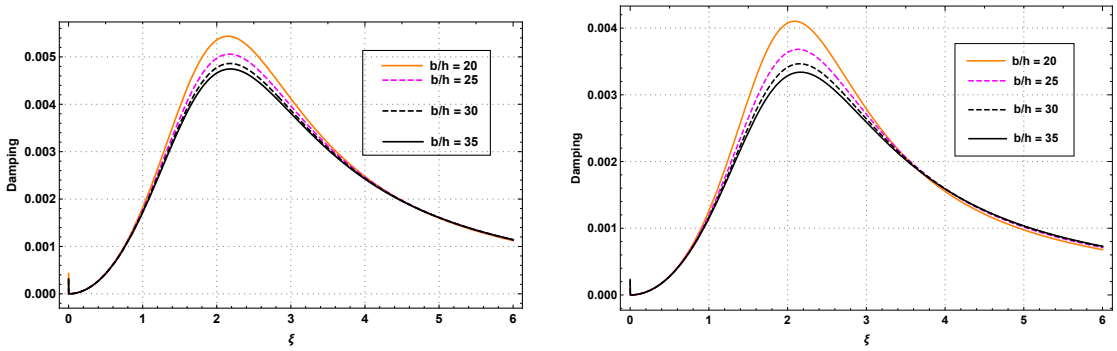

Figure 5.5.9: (a) Comparison of TED variation for different aspect ratios of $\frac{b}{h}$ corresponding to first mode. (b) Comparison of TED variation for different aspect ratios of $\frac{b}{h}$ corresponding to second mode.

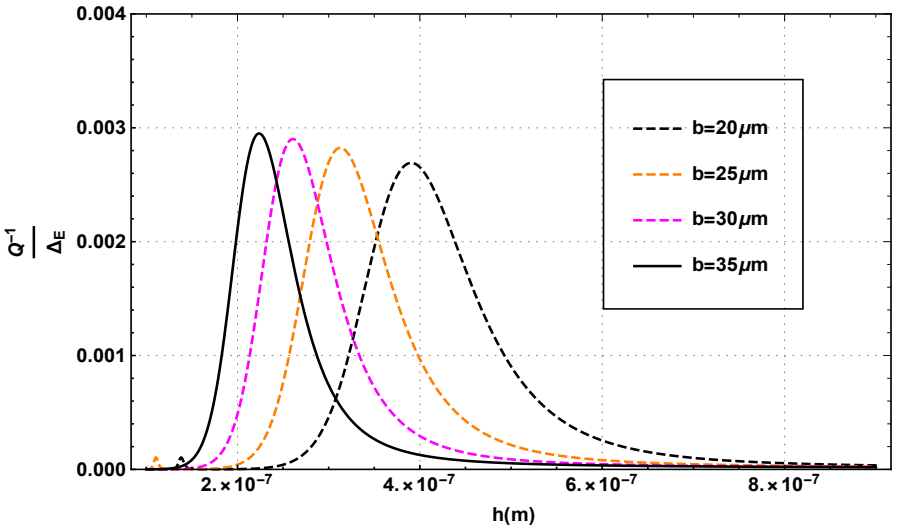

Figure 5.5.10: Comparison of TED variation with the function of plate thickness for different values of the width of the plate.

5.5.4 Effect of relaxation parameter on TED

Fig. 5.5.11 illustrates the variation of TED with the function of normalized variable ξ along with the first mode i.e., $(1, 1)$. This diagram demonstrates the importance of considering the relaxation parameter. With constant plate thickness $h = 6\mu m$ and increasing relaxation parameter, the peak of TED grows significantly. As can be seen here, increase in the relaxation parameter value, decreases QF dramatically. It's also possible to deduce that energy dissipation is slower when relaxation parameters are smaller. The GN-III model predicts a higher QF than the current MGT model, which is notable.

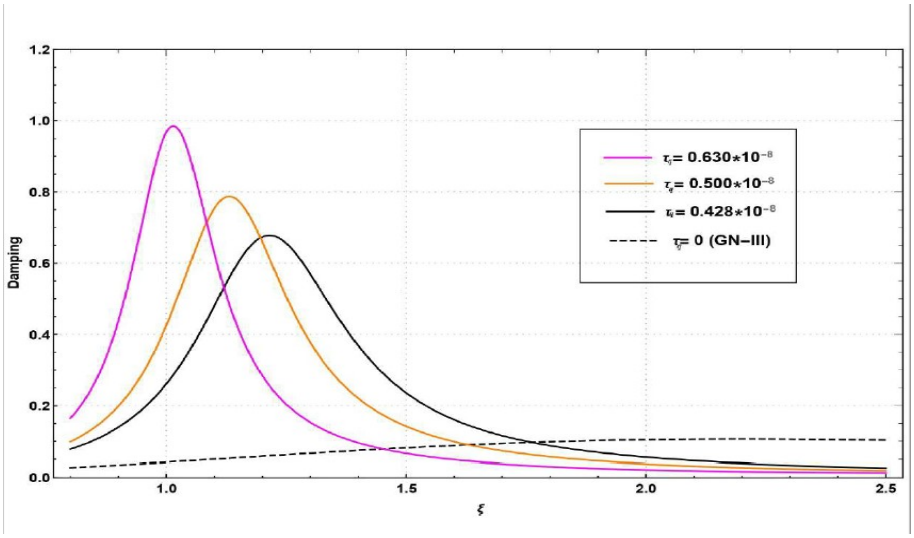

Figure 5.5.11: Comparison of TED variation with ξ at the first mode $(m = 1, n = 1)$ for distinct values of relaxation parameters τ_q.

5.5.5 Effect of plate thickness on TED

The impact of microplate thickness on TED as a function of length scale parameter considering different microplate thickness ($h = 6\mu m$, $8\mu m$, $10\mu m$ and $12\mu m$) is shown in Fig. 5.5.12. The curves are plotted for fixed plate length a ($a = 50\,\mu m$) and width b ($b = 30\,\mu m$). As expected, the influence of thickness of the plate resonator on damping is notable. In Fig. 5.5.12, a greater amount of TED is obtained at $h = 10\,\mu m$, although

less TED is exhibited at $h = 12\,\mu m$. Here, the non-monotonic behavior is characterized by distinct values of plate thickness h. Hence, it will be an arduous task to predict the thermoelastic nature of any rectangular structure due to its non-monotone behavior when dealing with the different plate thicknesses. By applying MCST to the plate resonator, similar findings are reported in works (Borjalilou and Asghari (2019), Kumar and Mukhopadhyay (2020)) for other thermoelastic model.

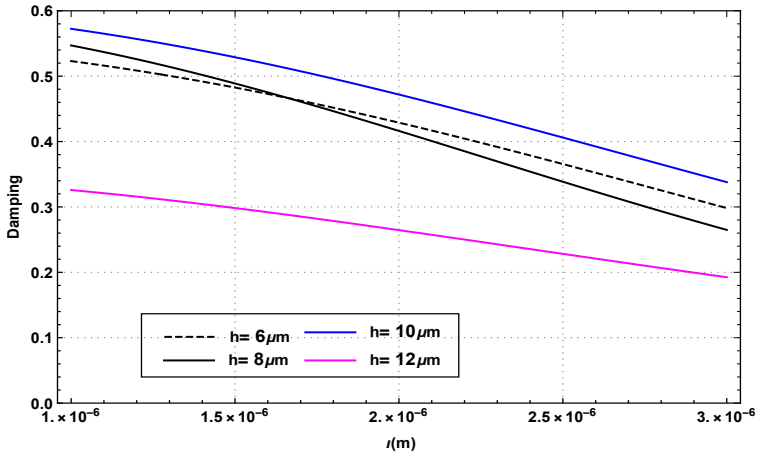

Figure 5.5.12: Comparison of TED with the function of material length scale parameter l for distinct microplate thickness.

5.5.6 Damping for different thermoelastic models

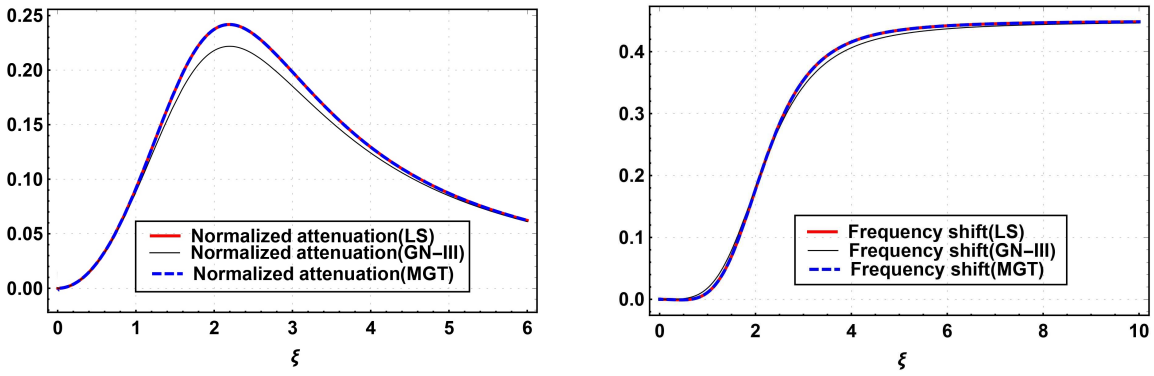

Figure 5.5.13: Normalized frequency shift and Normalized attenuation with respect to ξ for nonclassical thermoelastic models.

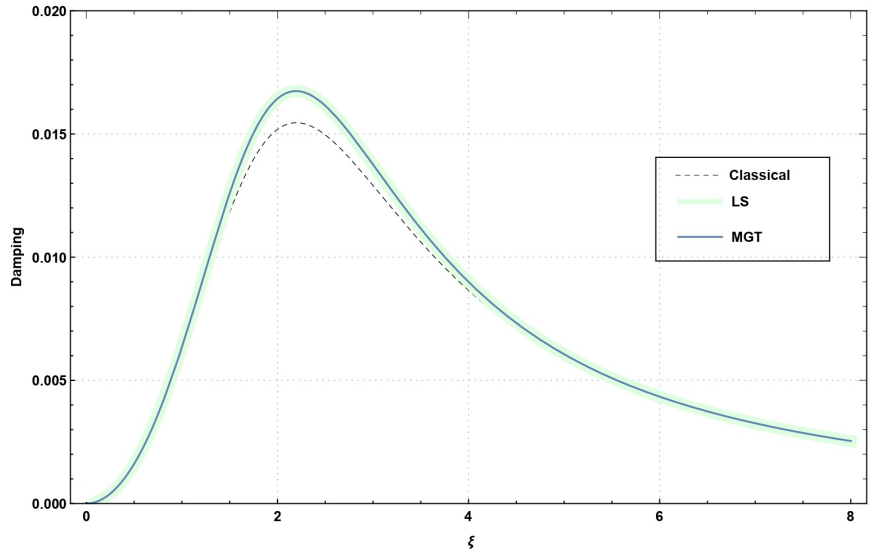

Figure 5.5.14: Damping with respect to ξ for classical and nonclassical thermoelastic models.

Figs. 5.5.13(a,b) represent the normalized frequency shift and normalized attenuation as function of ξ function and for three generalized thermoelastic models, namely, LS, GN-III, and MGT models. Here, the dimensions of the microplate resonator are fixed by setting length $a = 50\,\mu m$ with fixed material length scale parameter $l = 1\,\mu m$. The changes in normalized frequency shift and normalized attenuation under the MGT model are found to be identical to those seen under the LS model. These two generalized models attain their peak value at almost the same frequency, while energy dissipates as the frequency gets higher. As a result, clarifying the differences in variation between these two thermoelastic heat conduction models is challenging. Moreover, as seen in Figs. 5.5.13(a,b), the GN-III model calculates a lower values of frequency shift and normalized attenuation of TED than the MGT and LS models. It exhibits a prominent behavior of TED when compared with other two theories. Fig. 5.5.14 shows that the classical model has a higher quality factor, which is a significant factor in improved resonance performance.

5.6 Conclusion

Over the last decade, significant efforts have been put into developing size-dependent systems based on a higher-order continuum mechanics process. This Chapter provides an in-depth investigation of the development of the higher-order continuum theory for capturing size effects in small-sized structures. By employing the MCST and the MGT generalized thermoelasticity theory, the study of QF of TED in micro-sized thin Kirchhoff's plate resonator is discussed by frequency generation approach. The partial differential equations are solved by using an analytical method. For deriving the analytical expressions of QF, Hamilton's principle has been used to derive the governing equation of motion of the microplate under the plane stress condition. The analytical results are illustrated with a numerical example. The present results are further compared with the results of classical theory to delineate the small-scale size effects on the amount of TED based on various parameters. The numerical results allow us to draw the following conclusions:

- All estimations show that MCST produces lower TED values and better QF prediction than classical theory.

- When the frequency shift decreases, normalized attenuation decreases as well, and the QF increases.

- TED is reduced significantly when a dimensionless length scale parameter (l/h) is used to account for size effects.

- Microplates made of lead and silicon have the greatest and lowest TED values, respectively, when the TED values of copper, gold, silicon, and lead are compared. The TED for microplates made of copper and gold is in between the TED prediction for silicon and lead.

- When the width of microplate resonators is maintained constant, there is a significant variance in energy dissipation with aspect ratio of the plate, although the peak values of TED are attained to be almost the same.
- The QF decreases as the relaxation parameter in the MGT model is increased.
- TED delineates non-monotonic behavior as a function of plate thickness by keeping the phase-lag parameter constant.
- The results of the MGT model are more similar to the comparable results of the LS model, and the GN-III thermoelastic model predicts less thermoelastic attenuation and frequency shift than the MGT and LS models.